PAPER • OPEN ACCESS

Management of the correlations of UltracoldBosons in triple wells

New Journal of Physics
The open access journal at the forefront of physics

Deutsche Physikalische Gesellschaft DPG
IOP Institute of Physics

Published in partnership with: Deutsche Physikalische Gesellschaft and the Institute of Physics

OPEN ACCESS

RECEIVED
12 October 2018

REVISED
18 February 2019

ACCEPTED FOR PUBLICATION
20 March 2019

PUBLISHED
29 May 2019

PAPER

Management of the correlations of UltracoldBosons in triple wells

Sunayana Dutta[1], **Marios C Tsatsos**[2], **Saurabh Basu**[1] **and Axel U J Lode**[3,4]

[1] Department of Physics, Indian Institute of Technology Guwahati, Guwahati-781039, Assam, India
[2] São Carlos Institute of Physics, University of São Paulo, PO Box 369, 13560-970 São Carlos, São Paulo, Brazil
[3] Wolfgang Pauli Institute c/o Faculty of Mathematics, University of Vienna, Oskar-Morgenstern Platz 1, A-1090 Vienna, Austria
[4] Vienna Center for Quantum Science and Technology, Atominstitut, TU Wien, Stadionallee 2, A-1020 Vienna, Austria

E-mail: axel.lode@univie.ac.at

Keywords: Bose–Einstein condensate, fragmentation, cold atoms, optical potential

Supplementary material for this article is available online

Abstract

Ultracold interacting atoms are an excellent tool to study correlation functions of many-body systems that are generally eluding detection and manipulation. Herein, we investigate the ground state of bosons in a tilted triple-well potential and characterize the many-body state by the eigenvalues of its reduced one-body density matrix and Glauber correlation functions. We unveil how the interplay between the interaction strength and the tilt can be used to control the number of correlated wells as well as the fragmentation, i.e. the number of macroscopic eigenvalues of the reduced one-body density matrix.

1. Introduction

The successful experimental realization of Bose–Einstein condensation in gases of ultracold rubidium atoms in periodic potentials, so-called optical lattices [1, 2], has provided a powerful platform to study numerous exotic quantum many-body phenomena [3–5]. The dimensionality and depth of the wells of the lattice can be experimentally tuned to control the configuration of particles. Remarkably, also the atom-atom interactions can be tuned via Feshbach resonances [6–8].

Due to this impressive degree of experimental control, ultracold atoms in optical lattices can be used to mimic condensed matter systems and allow to simulate and probe their phase transitions [3, 9–12]. Additionally, direct imaging of quantum many-body correlations is feasible: one-, two-, and even many-body correlations have already been detected [13–16].

To assess and understand the many-body physics of interacting ultracold atoms in mesoscopic systems, it is a viable approach to first study and investigate their (few-body) building blocks [11, 17–20]. Here, we use a mesoscopic system of ultracold bosons in a triple-well potential as a candidate system to investigate the possibility for the control and manipulation of correlations in many-body systems. Some of their many-body aspects have been previously studied [21–23]; however, a scheme to control the emergent correlations still needs to be devised.

We work out such a protocol for the management of correlations by including the tilt of the optical lattice as a control parameter. A *tilted lattice* can routinely be achieved in the laboratory by superimposing a magnetic bias field to the optical potential. The inclusion of the tilt widens the spectrum of controllable parameters and enriches the emergent physics. For instance, Ising density-wave order and the appearance of superfluidity in transverse directions of a system of ultracold charged bosons confined in a lattice with a tilt were described in [24]. Reference [25] demonstrates that some eigenstates in the spectrum of neutral bosons confined in a tilted one-dimensional lattice exhibit localization and are robust against external perturbations. Furthermore, [26] shows that the tilt is a source of quantum decoherence for macroscopic quantum superpositions in ultracold atoms in a tilted well.

In this paper, we study the many-body correlations in the ground state of interacting ultracold bosonic atoms in a tilted triple-well potential by solving the corresponding Schrödinger equation using the multiconfigurational time-dependent Hartree for bosons (MCTDHB) approach.

We find and use the reduced density matrix (RDM) of the many-body state to quantify correlations. The system is said to be coherent and condensed if only one eigenvalue of the RDM is macroscopic [27] and is said to be correlated and fragmented if multiple eigenvalues of the RDM are macroscopic [28, 29]. To get a spatially resolved understanding of the emergent correlations, we compute the Glauber first-order correlation function from the RDM [30]. We study the emergence of correlations and fragmentation in the many-body system as a function of the interaction strength and the tilt of the triple well. Our results unravel an intriguing interplay between the tilt of the lattice potential and the strength of the interparticle interactions. We demonstrate how this interplay can be exploited to manage the correlations and fragmentation of many-boson systems in tilted optical lattices to a large extent.

The structure of the paper is as follows. Section 2.1 describes the many-body Hamiltonian, the form of the trapping potential along with the setup of the system. In section 2.2, we briefly discuss the basics of MCTDHB. We introduce the quantities of interest, namely, the one-body RDM and the first-order correlation function, that is extensively used for this work in section 2.3. In section 3 we present our results, on the ground state properties of a system of bosons in tilted triple wells. Precisely, we find the natural occupations (section 3.1), the correlations between the bosons of different wells (sections 3.2, 3.3) and the behavior of the natural orbitals (section 3.4). Conclusions and an overview are presented in section 4.

2. Method, setup, and quantities

The properties of ultracold bosonic many-body systems are described by the time-dependent many-body Schrödinger equation for interacting and indistinguishable bosonic particles. Commonly, the many-body problem is solved by the mean-field Gross–Pitaevskii approximation [31, 32] or the Bose–Hubbard (BH) model [3, 12]. In the Gross–Pitaevskii picture the RDM has only a single eigenvalue and hence correlations and fragmentation—pivotal in the superfluid to Mott-insulator phase transition [3, 12]—cannot be captured. In the BH model a fixed basis set of Wannier (or Wannier–Stark) states is utilized [33–35]. Albeit being an apt choice for regular lattices, a Wannier basis may not be optimal for tilted lattices because the tilt renders the shape of the site-local single-particle states different from Wannier functions.

While generalizations within the BH model rely on multi-band or Wannier–Stark single-particle basis sets, we go here beyond the BH models and employ the optimized single-particle basis given by MCTDHB. The optimized MCTDHB basis has been demonstrated to be far more accurate than non-optimized basis sets [36]. The MCTDHB theory optimizes variationally both the basis set *and* the expansion coefficients in that basis set (see [37, 38] and references therein); its solutions thus assume no predetermined symmetry or shape of the described many-body state. Therefore, we use MCTDHB to obtain an optimized problem-adapted basis to investigate tilted lattices. MCTDHB is in principle exact [36, 39], has been verified with experimental results [40], can describe both coherent and fragmented condensates, and includes the GP theory as an extreme case when only one single-particle state is considered; see [38, 41, 42] for details on MCTDHB.

2.1. Hamiltonian

The N-boson state $|\Psi\rangle$ is governed by the time-dependent Schrödinger equation

$$\mathrm{i}\partial_t|\Psi\rangle = \hat{H}|\Psi\rangle, \tag{1}$$

with the Hamiltonian

$$\hat{H}(x_1, x_2, \ldots, x_N) = \sum_{j=1}^{N} \hat{h}(x_j) + \sum_{k>j=1}^{N} \hat{W}(|x_j - x_k|). \tag{2}$$

We compute the ground state of the Hamiltonian in equation (2) by propagating equation (1) in imaginary time to damp out any excitation in the one-dimensional many-body system. Here, x_j represents the position of the jth boson, $\hat{h}$ is the single-particle Hamiltonian $\hat{h}(x) = \hat{T}(x) + \hat{V}_{\mathrm{trap}}(x)$; $\hat{T}(x)\left(=-\frac{\hbar^2}{2m}\frac{\partial^2}{\partial x^2}\right)$ and $\hat{V}_{\mathrm{trap}}(x)$ are the usual kinetic and external potential energy, respectively. Interactions of ultracold dilute bosonic gases are typically modeled using a Dirac-delta distribution: $\hat{W}(x_j - x_k) = \lambda_0\delta(x_j - x_k)$. Here, λ_0 is referred to as the strength of interactions. We scale λ_0 with the particle number as $\lambda = \lambda_0(N-1)$. In equations (1), (2) and the remainder of this work dimensionless units are employed. To define dimensionless units, we divide the Hamiltonian by $\hbar^2/(mL^2)$, where m is the mass of the considered boson and L a convenient length scale. We first choose a length scale of $L = 1\ \mu$m. The scale of energy for the mass of ^{87}Rb is $\hbar^2/(mL^2) = 2\pi\hbar \times 116$ Hz and the scale of time is $mL^2/\hbar = 1.37$ ms. The one-dimensional scattering parameter λ is related to the

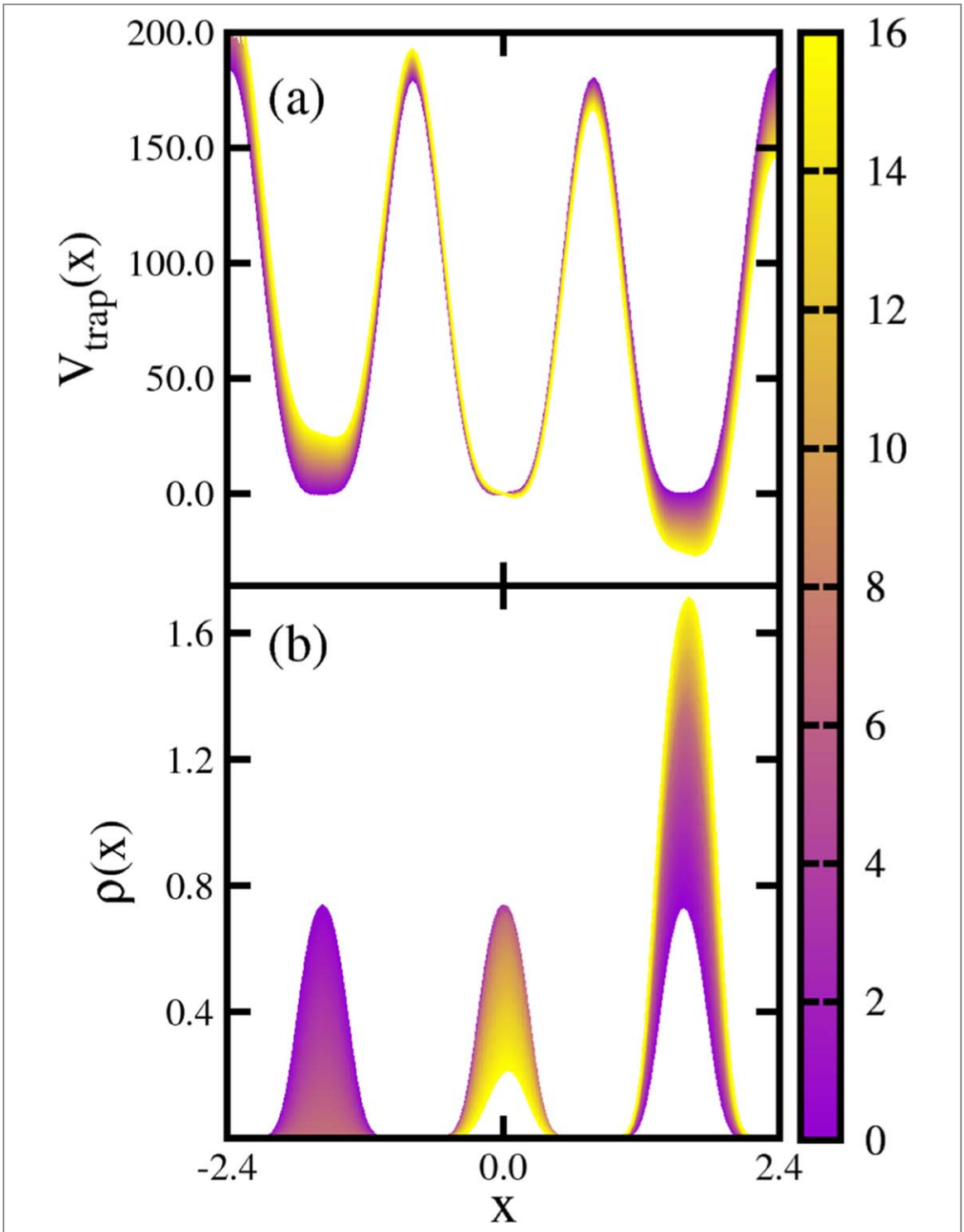

Figure 1. Potential and density as a function of the tilt. (a) shape of the triple well $V_{\rm trap}(x)$ for $V_0 = 180$, $\lambda = 6$ and various tilts α and (b) corresponding density $\rho(x)$ for the same α, ranging from $\alpha = 0$ to $\alpha = 16$ (see color code/gray-scale).

three-dimensional scattering length a_{3D} by $\lambda = 2Lm\omega_\perp a_{3D}/\hbar$, where $\omega_\perp$ is the frequency of the transversal confinement [43]. Using $a_{3D} = 100.4a_0$, where a_0 is the Bohr radius, and $\lambda = 6$ ($\lambda = 20$), one obtains $\omega_\perp = 41.3$ kHz ($\omega_\perp = 1376$ kHz).

We consider $N = 90$ interacting bosons in a trap of the form

$$V_{\rm trap}(x) = -\alpha x + V_0 \sin^4(kx) + f_w(x). \tag{3}$$

Here α is the tilt and V_0 the barrier height. We fix $k = 2$ for the lattice spacing. The term $f_w(x)$ introduces quasi-hard-wall boundary conditions. The tilt αx renders the trapping potential similar to that of charged particles in a constant electric field and can be realized by applying a magnetic field gradient to ultracold neutral bosons in a lattice. We note the possibility of achieving, virtually, any periodic lattice in the experiment [44]. The potential is plotted in figure 1(a) for $\alpha \in [0,16]$.

2.2. Method: the multiconfigurational time-dependent Hartree method for bosons (MCTDHB)

The key idea of the MCTDHB approach is the use of time-adaptive basis states. The bosonic field operator which annihilates a particle at position x is represented by a set of M orthonormal, time-dependent functions (orbitals) $\{\varphi_i(x, t)\}$

$$\hat{\Psi}(x,\ t) = \sum_{i=1}^{M} \hat{a}_i \varphi_i(x,\ t). \tag{4}$$

Here, the bosonic creation and annihilation operators $\hat{a}_i,\ \hat{a}_i^\dagger$ obey the usual commutation relations at any instant t.

The ansatz for the many-boson wave function assumed in MCTDHB is

$$|\Psi(t)\rangle = \sum_{\vec{n}} C_{\vec{n}}(t)|\vec{n};\ t\rangle. \tag{5}$$

Here, the summation runs over all possible configurations $\{\vec{n} = (n_1, \ldots, n_M)\}$, for which $\sum_i n_i = N$. Thus N bosons are distributed over M accessible orbitals. Using the bosonic creation operators $\{\hat{a}_k^\dagger\}$, the time-dependent configurations can be written as

$$\begin{aligned}|\vec{n};\ t\rangle &= \frac{[a_1^\dagger(t)]^{n_1}[a_2^\dagger(t)]^{n_2}\ldots[a_M^\dagger(t)]^{n_M}}{\sqrt{n_1!n_2!n_3!\ldots n_M!}}|0\rangle \\ &\equiv |n_1,\ n_2,\ n_3,\ldots n_M;\ t\rangle.\end{aligned} \tag{6}$$

Here, $|0\rangle$ is the vacuum state. Since the permanents $|n_1, \ldots, n_M;\ t\rangle$ are a complete basis set of N-body Hilbert space for $M \to \infty$, the variational principle [45] guarantees that the solutions of the time-dependent many-body problem provided by the MCTDHB method gradually improve towards exactness when the number of considered creation operators M in the ansatz, equation (5), is increased [36, 39]. To derive the MCTDHB equations, the time-dependent variational principle [45] is employed to determine the time-evolution of the expansion coefficients $\{C_{\vec{n}}(t)\}$ and the orbitals $\{\varphi_i(\mathbf{r},\ t)\}$ [37, 38]. The MCTDHB equations are obtained by fixing a gauge freedom in the choice of the orbitals by the condition $\langle\frac{\partial\varphi_j}{\partial t}|\varphi_i\rangle = 0,\ \forall j,\ i \in [1,\ M]$.

In Lagrangian formulation, the functional action of the time-dependent Schrödinger equation [with many-body ansatz, equation (5)] reads as [37, 38]

$$S[\{C_{\vec{n}}(t)\},\ \{\varphi_i(\mathbf{r},\ t)\}] = \int \mathrm{d}t\,\{\langle\Psi|\hat{H} - i\frac{\partial}{\partial t}|\Psi\rangle - \sum_{i,j=1}^{M}\mu_{ij}(t)[\langle\varphi_i|\varphi_j\rangle - \delta_{ij}]\}. \tag{7}$$

To ensure that the time-dependent orbitals remain orthonormal during the propagation, time-dependent Lagrange multipliers $\mu_{ij}(t)$ have been introduced here.

The variation of the action with respect to the expansion coefficients $C_{\vec{n}}(t)$ yields the equations of motion for the expansion coefficients [37, 38]

$$\sum_{\vec{n}} \mathcal{H}_{\vec{n}\vec{n}'}(t)C_{\vec{n}} = i\frac{\partial C_{\vec{n}'(t)}}{\partial t}. \tag{8}$$

This equation of motion is a first-order differential equation and the matrix $\mathcal{H}_{\vec{n}\vec{n}'}(t) = \langle\vec{n};\ t|\hat{H}|\vec{n}';\ t\rangle$ is time-dependent as the permanents $|\vec{n};\ t\rangle$ and $\hat{H}$ itself are functions of time.

The variation of the action with respect to the orbitals $\{\varphi_i(x, t)\}$ yields the equation of motion for the orbitals [37, 38]:

$$i|\ \dot{\varphi}_i\rangle = \hat{\mathbf{P}}\left[\hat{h}|\ \varphi_i\rangle + \sum_{k,s,q,l=1}^{M}\{\boldsymbol{\rho}(t)\}^{-1}_{ik}\rho_{ksql}\hat{W}_{sl}|\ \varphi_q\rangle\right], \tag{9}$$

where

$$\hat{\mathbf{P}} = 1 - \sum_{i'=1}^{M}|\varphi_{i'}\rangle\langle\varphi_{i'}| \tag{10}$$

is a projector, $\rho_{jk} = \langle\Psi|\hat{a}_j^\dagger\hat{a}_k|\Psi\rangle$ are the matrix elements of the one-body RDM, and $\rho_{ksql} = \langle\Psi|\hat{a}_k^\dagger\hat{a}_s^\dagger\hat{a}_l\hat{a}_q|\Psi\rangle$ are the matrix elements of the two-body RDM. The local interaction potentials read $\hat{W}_{sl} = \int \mathrm{d}x'\varphi_s^*(x',\ t)\,W(x,\ x')\varphi_l(x',\ t)$. For the contact interactions that we consider in the main part of this paper, the $\hat{W}_{sl}$ are given by $\hat{W}_{sl} = \lambda_0\varphi_s^*(x,\ t)\varphi_l(x,\ t)$.

The MCTDHB thus yields descriptions of many-boson systems that allow for correlations to be intrinsically described without any *a priori* requirements. Coherent systems (states whose one-body RDM has a single contributing eigenvalue) [27] and fragmented systems (states whose one-body RDM has several macroscopic eigenvalues) [28, 29] can be described by MCTDHB alike [46–50].

Notably, when $M = 1$ is set in equation (5) the MCTDHB ansatz becomes identical to the wavefunction ansatz of the time-dependent Gross–Pitaevskii (TDGP) theory and, consequently, the MCTDHB equations of motion boil down to the TDGP equation. For further details about the MCTDHB method see [37, 38, 41].

MCTDHB represents a generalization beyond exact diagonalization approaches with static basis sets like the Bose–Hubbard approach that uses Wannier functions. Necessarily, the self-consistent basis of MCTDHB is superior to a fixed static (Wannier) basis as shown directly in [36, 39, 51–54].

Since our focus in this work is on the physics of the ground state of interacting bosons in a tilted triple well potential, we will, for the sake of brevity, omit indicating the explicit time-dependence of quantities in the following. The ground states that we discuss in the following were obtained by propagating the coupled MCTDHB equations [equations (8), (9)] in imaginary time to damp out all excitations.

2.3. Quantities of interest

The one-body RDM of the N-boson state $|\Psi(t)\rangle$ is defined as:

$$\rho^{(1)}(x, x') = \langle\Psi|\hat{\Psi}^{\dagger}(x')\hat{\Psi}(x)|\Psi\rangle = \sum_i n_i \phi_i^*(x')\phi_i(x), \tag{11}$$

in its eigenbasis $\{\phi_i(x)\}$ [55, 56]. Here n_i is the ith eigenvalue and $\phi_i(x)$ the corresponding eigenfunction, also known as natural occupation and natural orbital, respectively. The diagonal $\rho^{(1)}(x, x)$ is the single-particle probability distribution $\rho(x)$. A BEC is condensed if its RDM has only a single macroscopic eigenvalue [27] and k-fold fragmented, if its RDM has k macroscopic eigenvalues [28, 29]. The first-order coherence of a condensed state is maintained everywhere in space. Therefore, the value of the first occupation $\frac{n_1}{N} \approx 1$ ($\frac{n_1}{N} < 1$) is also indicative of the (loss of) coherence of the state [see equation (12) below].

To obtain a spatially resolved picture of the correlations between the atoms in the many-body state that are triggered by a specific trap geometry, we study the behavior of the first-order correlation function,

$$|g^{(1)}(x, x')|^2 = \left| \frac{\rho^{(1)}(x, x')}{\sqrt{\rho^{(1)}(x, x)\rho^{(1)}(x', x')}} \right|^2. \tag{12}$$

The value $|g^{(1)}(x, x')|^2$ marks the first-order coherence between the points x and x' ($|g^{(1)}(x, x')|^2 \approx 1$) or its absence ($|g^{(1)}(x, x')|^2 \approx 0$) in the state $|\Psi\rangle$ [30]. Here, the system of atoms is said to be in a coherent state if $|g^{(1)}(x, x')|^2 \approx 1$, similarly it is said to be in an incoherent state when $|g^{(1)}(x, x')|^2 \approx 0$.

In the following discussion for first-order correlation (see section 3.2), we use the term *inter-well coherence* if x is in the vicinity of a different minimum of V_{trap} than x' and $|g^{(1)}(x, x')|^2 \approx 1$ holds. Moreover, we use the term *intra-well coherence* if $|g^{(1)}(x, x')|^2 \approx 1$ holds for coordinates x and x' that are both in the vicinity of the same minimum.

3. Results

For our numerical calculations, we use $M = 3$ one-dimensional single-particle basis functions and consider $N = 90$ particles. We also tested $M > 3$ for convergence and checked the consistency of our results with a potential where we replace the $\sin^4(kx)$ term in equation (3) by[5] $\sin^2(kx)$. For the present computations we use the MCTDH-X implementation of the MCTDHB theory [41, 42, 57]. For the following simulations we set the quasi-hard-wall boundaries as $f_w(x) = \left(\frac{x}{x_c}\right)^{60}$ and $x_c = \frac{3\pi}{2k} - \frac{1}{k}$ to define the effective extension of the triple well. Our numerical grid runs from $x_{\min} = -x_c - 1.09/k$ to $x_{\max} = x_c + 1.09/k$ and we use 256 grid points.

We start our investigation by plotting the one-body density $\rho(x)$ as a function of the tilt α in figure 1(b) as a function of the tilt α. The effect of the tilt on the density $\rho(x)$ is intuitive: as α increases the density of the atoms is gradually forced downhill and $\rho(x)$ is localized mostly at the rightmost well where the potential energy is minimal for $\alpha > 0$.

We chose the values of the interaction strength ($\lambda = 6$) and barrier height ($V_0 = 180$) such that the ground state is threefold fragmented in the absence of tilt ($\alpha = 0$). To assess the impact of the barrier height and the interaction strength on the properties of the many-body state, we additionally consider a larger interaction strength, namely $\lambda = 20$, and a moderate barrier height, namely $V_0 = 80$.

[5] See supplemental material is available online at stacks.iop.org/NJP/21/053044/mmedia at [URL] which includes a description of the MCTDHB approach and its convergence, a discussion of the (in-)applicability of a Hubbard description, as well as complementary results on the correlations and the occupation numbers as a function of barrier height and interaction strength for short- and long-range interactions.

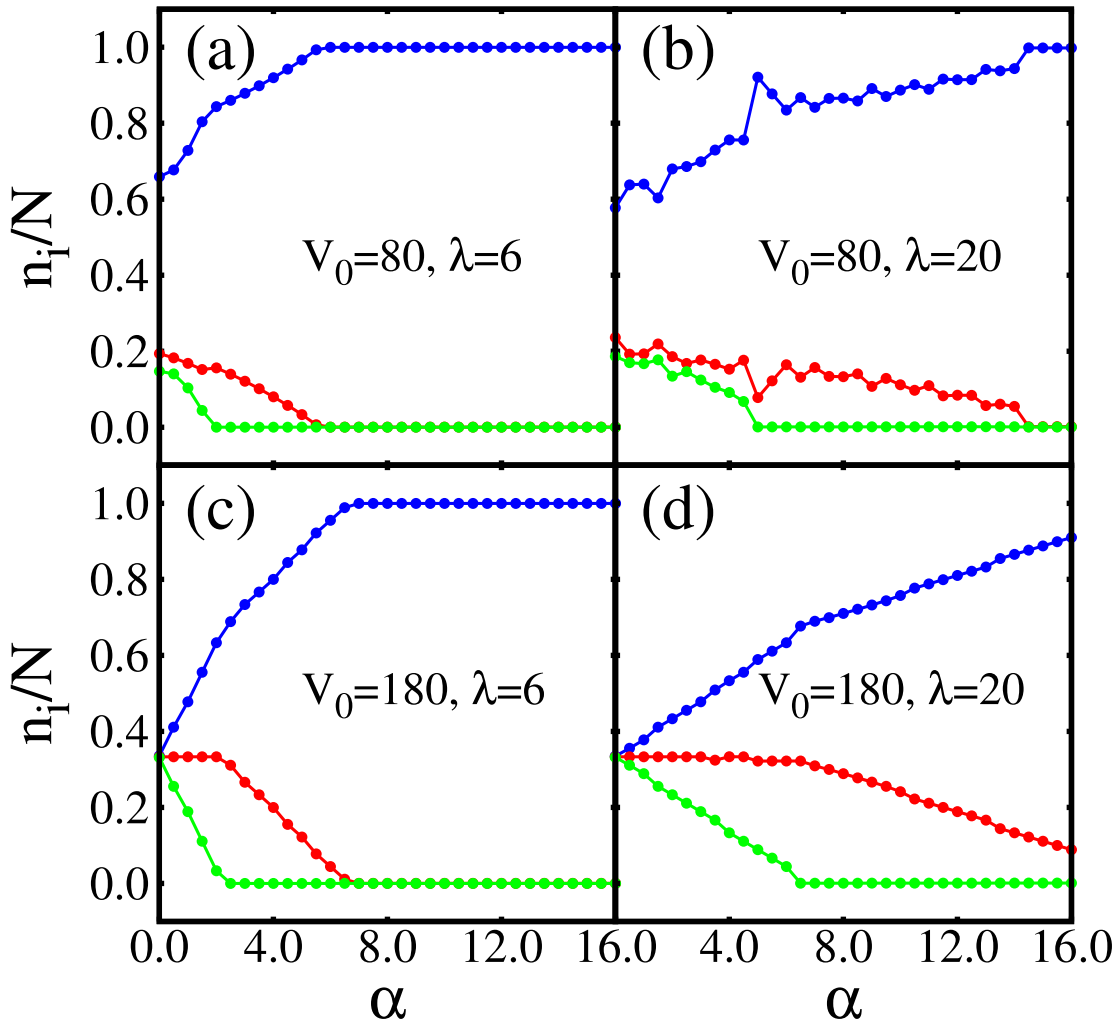

Figure 2. Fragmentation as a function of the tilt of the lattice. The natural occupations $\frac{n_i}{N}$ are shown as a function of the tilt α for barrier heights $V_0 = 80$ [$V_0 = 180$] in (a), (b) [(c), (d)]. Panels (a), (c) [(b), (d)] correspond to interaction strength $\lambda = 6$ [$\lambda = 20$]. In all panels, the blue line with circles represents $\frac{n_1}{N}$, the red line with circles represents $\frac{n_2}{N}$, and the green line with circles represents $\frac{n_3}{N}$. For all depicted parameters, fragmentation gradually diminishes with increasing tilt α; for large tilts, the state hence becomes coherent and the occupation numbers obtained are $\frac{n_1}{N} \approx 1$; $\frac{n_2}{N} \approx \frac{n_3}{N} \approx 0$. All quantities shown are dimensionless, see text for further discussion.

3.1. Natural occupations

To quantify the fragmentation, coherence, and correlation properties of the many-boson system we discuss the behavior of the natural occupations, $\frac{n_i}{N}$, as a function of the tilt α [equation (3)], see figure 2.

For moderate barrier height, $V_0 = 80$, and no tilt, $\alpha = 0$, the bosons are not completely fragmented, i.e. $\frac{n_1}{N} > 60\%$ and $\frac{n_{2,3}}{N} < 20\%$, for both small and large interaction strengths ($\lambda = 6$ and $\lambda = 20$). This is in contrast to the entirely threefold fragmented state found for $V_0 = 180$ with $\frac{n_1}{N} \approx \frac{n_2}{N} \approx \frac{n_3}{N} \approx 33.33\%$ [see figure 2, panels (a), (b) and figure 2, panels (c), (d)]. We conclude that, at zero tilt, fragmentation can be tuned by the barrier height alone. As α grows larger so does the first natural occupation, $\frac{n_1}{N} \to 1$, while the other two natural occupations decrease, i.e. $\frac{n_{2,3}}{N} \to 0$, see figures 2(a) and (b).

At large barriers, $V_0 = 180$, and moderate interactions $\lambda = 6$, the state exhibits threefold fragmentation at $\alpha = 0$. As α increases past a threshold value of $\alpha \approx 7.5$, the state becomes coherent with $\frac{n_1}{N} \approx 1$, $\frac{n_2}{N} \approx \frac{n_3}{N} \approx 0$, see figure 2(c). Interestingly, the second natural occupation $\frac{n_2}{N}$ remains constant up to tilts as large as $\alpha \approx 2$, while $\frac{n_3}{N}$ starts to drop from $\frac{1}{3}$ to 0 already at $\alpha \approx 0$. For $\alpha > 2$, n_2 falls off gradually and vanishes at $\alpha \approx 7.5$ [see figure 2(c)]. Beyond this tilt the density is almost exclusively localized in the rightmost well. For larger barriers, $V_0 = 180$, and moderate interactions, $\lambda = 6$, an increasing tilt α thus triggers a transition from a fully threefold fragmented to a fully condensed state, i.e. the tilt can be used to control fragmentation.

For larger interactions, $\lambda = 20$, and a large barrier height, $V_0 = 180$, the transition between a fragmented and a depleted state is still found, however, at larger tilts α [compare figures 2(c) and (d)].

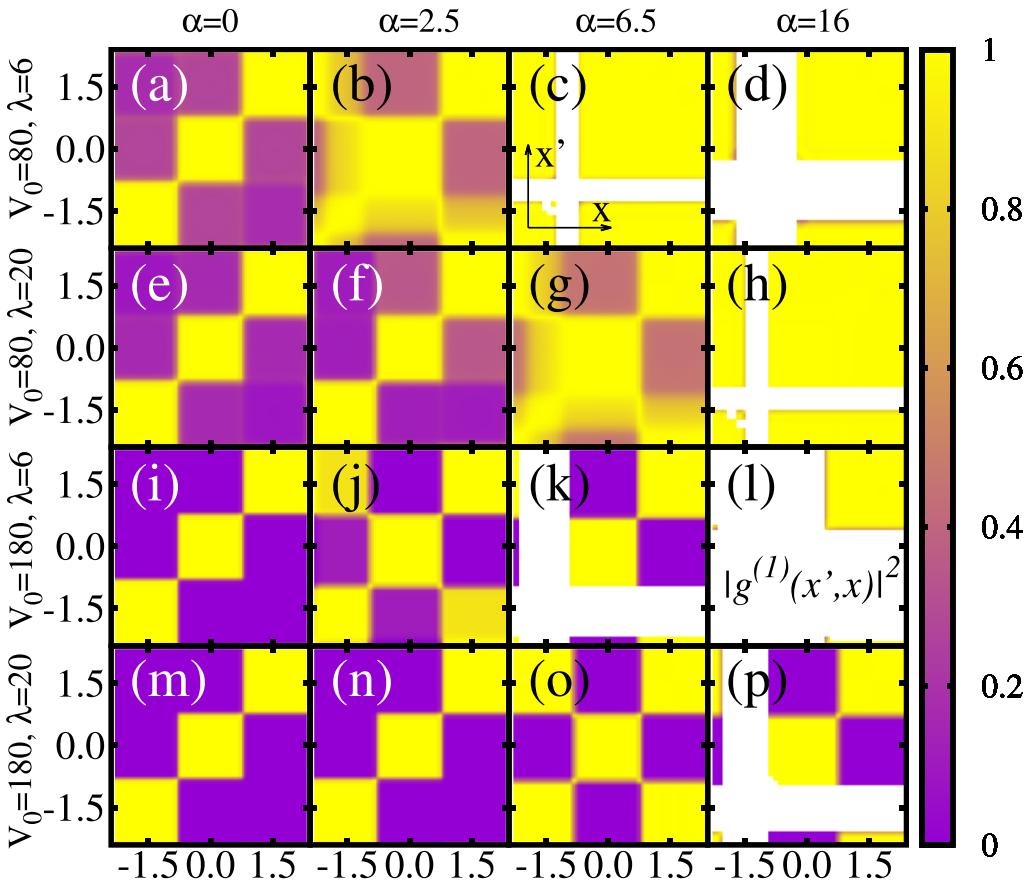

Figure 3. Spatially tracing correlations between the bosons in the triple well as a function of the tilt and barrier height. The first-order normalized correlation function $|g^{(1)}(x',\, x)|^2$ is visualized as a function of α wherever the density is larger than a threshold value, i.e., where $\rho^{(1)}(x, x) > 0.01$ and $\rho^{(1)}(x',\, x') > 0.01$. See labels for the respective values of the barrier height V_0 and the tilt α. We infer that an increased repulsion between the bosons, postpones changes in the coherence to larger tilts; see the similarity of panels (b) and (g), (c) and (h) for $V_0 = 80$ and of panels (j) and (o), (k) and (p) for $V_0 = 180$. See text for discussion.

We have verified that the above findings for the natural occupations and the fragmentation of the state also hold for the case of long-range interactions of the form $\hat{W}(r_j - r_k) = \lambda_0/(|x_j - x_k|^3 + \Delta^3)$ [58–60, 61]. The natural occupations follow the same pattern as their contact-interaction counterparts, but the restoration of coherence seems to happen at even larger values α as compared to the case of contact interactions. This demonstrates the sharper effect of long-range interactions on the fragmentation, see supplemental material[5]. We thus conclude that the tilt of the triple well can be used to tune the many-body state from fragmented to condensed.

3.2. First-order correlation

To get a spatially resolved picture of the correlations between the atoms, we plot the first-order correlation function, $|g^{(1)}|^2$ [as defined in equation (12)] for various tilts ($\alpha = 0, 2.5, 6.5, 16$), barrier heights ($V_0 = 80, 180$) and interaction strengths ($\lambda = 6, 20$) in figure 3.

We first discuss the correlation function for a moderate barrier height, $V_0 = 80$, in figures 3(a)–(h). At a small interaction strength ($\lambda = 6$), coherence between different wells persists since $|g^{(1)}(x,\, x')|^2$ is significantly larger than zero at off-diagonal values $x \neq x'$ for all tilts, figures 3(a)–(d). For larger interaction strengths ($\lambda = 20$), inter-well coherence is absent for no tilt ($\alpha = 0$), figure 3(e). As the tilt increases, inter-well coherence between populated neighboring wells is gradually restored, see figures 3(a)–(d) for $\lambda = 6$ and figures 3(f)–(h) for $\lambda = 20$: $|g^{(1)}(x,\, x')|$ gradually grows towards unity for values $x \neq x'$. We note that a tilt-driven localization takes place for larger tilts: for tilts $\alpha \gtrsim 10$, the left well contains almost no particles [see figure 1(b)].

The effect of interactions is to merely diminish the inter-well coherence, see figures 3(a)–(d) and (e)–(h): the value of $|g^{(1)}(x,\, x')|^2$ is generally closer to unity on the off-diagonal $x \neq x'$ for small interactions [figures 3(a)–(d)] as compared to larger interactions [figure 3(e)–(h)].

We now turn to an analysis of the details of the spreading of the coherence. Two competing tendencies are observed in the evolution of coherence as a function of the tilt α that can be illustrated with panels (a), (b), (e), (f), (g) of figures 3: tendency **I.** is an increase of the coherence between the center and the right well with the tilt see

figures 3(a) to (b), and figures 3(e) to (f), respectively. Tendency **II.** is the restoration of coherence between the central and the left well. Both, tendency **I.** and **II.** can be understood by the following consideration about the behavior of interaction and interaction energy as a function of increasing tilt α: naturally, an increase of α forces the particles downhill and the density gradually accumulates more in the right well, depleting the central and the left well (see also figure 1). This leads to an interaction induced broadening of the density in the right well, because the presence of more particles implies a larger local portion of interaction energy; thus, due to the tilt, the density in the right well penetrates more into the potential barrier between central and the right well and, thereby, increases the tunneling between these wells—hence the partial revival of coherence between the central and right well is seen going from figure 3(a) to (b) and going from figure 3 (e) to (f). Tendency **II.**, the restoration of coherence between the left and central wells going from figure 3(a) to (b) or, equivalently, from figure 3(f) to (g), can also be understood as a consequence of the tilt-driven migration of interaction energy towards the right well: since the central and left wells are gradually depleted, the local contribution to the interaction energy is decreasing there. The coherence between the left and central well is restored [figures 3(b) and (g)], when the subsystem remaining in these wells is effectively non-interacting and its 'local' state is well-described by a product of a single complex-valued function.

We note here that we verified that the above tendency **I.** starts affecting the correlation patterns at smaller tilts than the tendency **II.** not only for $\lambda = 20$, $V_0 = 80$ [see change from figure 3(e) to (f)], but also for $\lambda = 6$, $V_0 = 80$: for tilts $\alpha \lesssim 1.5$ with $V_0 = 80$ and $\lambda = 6$, the correlation pattern (not shown) closely resembles the one depicted in panel (f) of figure 3 for $\lambda = 20$ and $V_0 = 80$.

We thus demonstrate that an increase of the tilt, at a fixed interaction strength, assists inter-well coherence of bosons in neighboring wells, while an increase of the interaction strength, for fixed moderate barrier heights, diminishes inter-well coherence (section 3.3).

We now analyze the correlations for larger barrier heights ($V_0 = 180$), figures 3(i)–(p). For zero tilt and in comparison to moderate barrier heights, inter-well coherence is completely lost at large barrier heights, $|g^{(1)}(x, x') \approx 0|^2$ for $x \neq x'$ in figures 3(i), (m).

By comparing the correlations at moderate barrier heights to the correlations at larger barrier heights, we find—as expected—that a larger value of V_0 increases the degree of localization of the system. This is true, independently of the interparticle interaction strength; compare first and third as well as second and fourth row of figure 3.

Similarly to moderate barrier heights, a restoration of coherence is also seen as the tilt α is increased for larger barriers V_0. This restoration of coherence is followed by a revival of next-to-nearest-neighbor-coherence to a smaller degree [see figures 3(b) and 3(g)] in the case of moderate barriers. For large barriers, however, the revival of the next-to-nearest-neighbor-coherence is much more prominent, while the nearest neighbors remain incoherent, see figure 3(j) for weak interactions and figure 3(o) for strong interactions.

Note that we have checked the persistence of the revival of next-to-nearest-neighbor coherence at a larger accuracy, i.e. for $M = 4$ orbitals. We found that the effect appears at larger tilts ($\alpha = 7.1$) for the case of $M = 4$. We therefore speculate that the next-to-nearest neighbor coherence results from a resonance condition involving two- or many-particle correlated tunneling processes [39, 62, 63]; the lowered energy at the $M = 4$-level of MCTDHB (footnote 5) seems to cause the resonance condition to be fulfilled at a different tilt.

The effect of stronger interactions is, one, to defer the restoration of coherence to larger tilts (from $\alpha = 2.5$ for $\lambda = 6$ to $\alpha = 6.5$ for $\lambda = 20$) and, two, to shift the tilt-driven localization of the bosons to larger tilts. For strong interactions, $\lambda = 20$, at $\alpha = 16$ two wells are populated and at $\alpha = 6.5$ three wells are populated. For weak interactions, $\lambda = 6$, in contrast, only one well is populated at $\alpha = 16$ and two wells are populated at $\alpha = 6.5$.

We assess the generality of our findings for the coherence properties for long-range interactions in the supplemental material (footnote 5). The inclusion of long-range interactions favors the fragmentation of the BEC for a larger barrier height. We find that our main conclusions for short-ranged interactions hold also for the case of long-ranged interactions.

3.3. Inter-well correlation

The left-right inter-well correlation can be defined as:

$$|g^{(1)}(x_l, x_r)|^2 = \left| \frac{\rho^{(1)}(x_r, x_l)}{\sqrt{\rho^{(1)}(x_r, x_r)\,\rho^{(1)}(x_l, x_l)}} \right|^2 . \tag{13}$$

The quantity $|g^{(1)}(x_l(\alpha), x_r(\alpha))|^2$ gives the degree of first-order correlation between points $x = x_r(\alpha)$ and $x' = x_l(\alpha)$. For our potential, equation (3), the position $x_r(\alpha)$ [$x_l(\alpha)$] of the right [left] well minimum is weakly dependent on the tilt α. The right [left] well extends from about 1.5–2.1 [-1.5 to -2.1] for the considered tilts α. We plot the inter-well correlations as a function of the tilt α for various barrier heights V_0 and interaction strengths λ in figure 4.

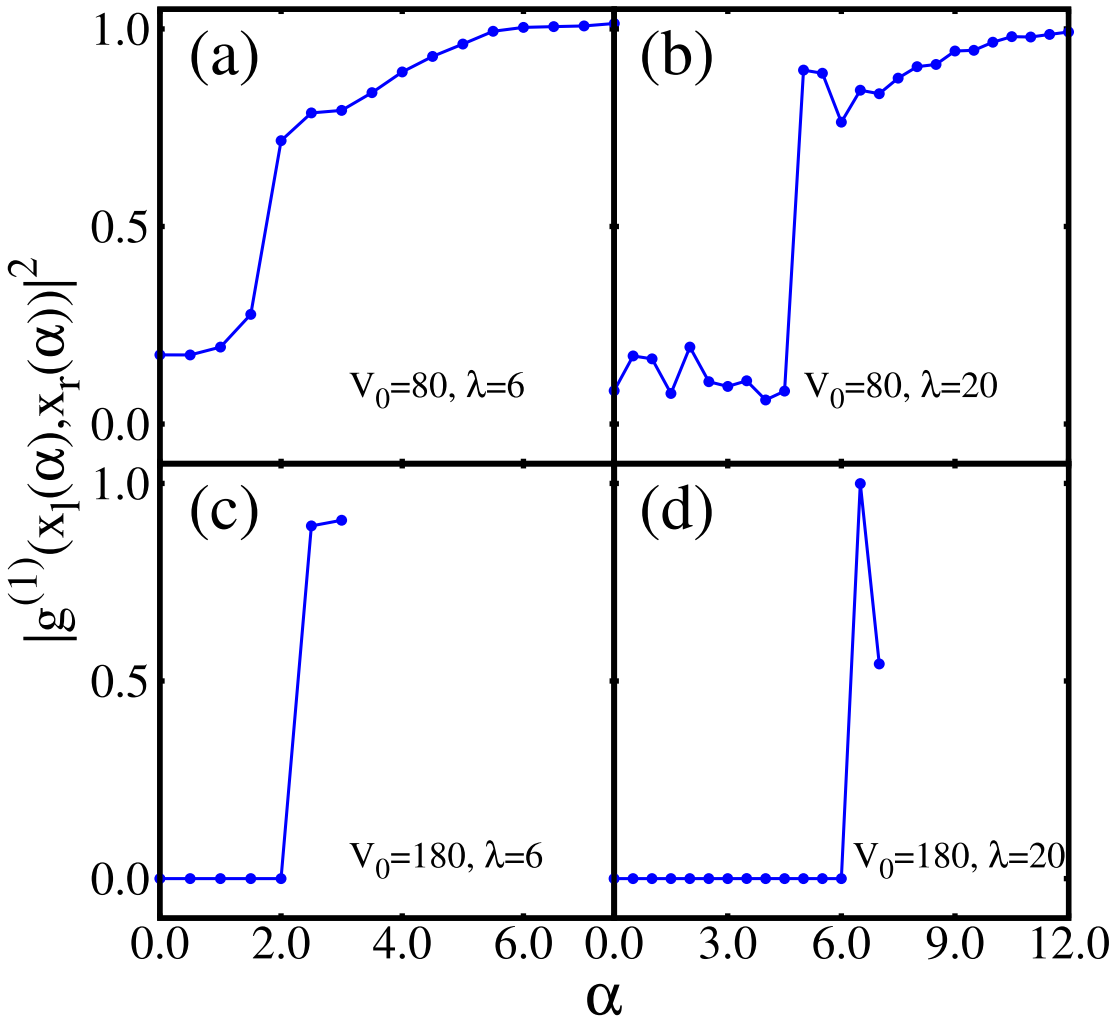

Figure 4. Behavior of the first-order inter-well correlation function, $|g^{(1)}(x_l(\alpha),\ x_r(\alpha))|^2$, for varying barrier height and interaction strength for various values of α. (a) and (b) correspond to $\lambda = 6$ and $\lambda = 20$ for $V_0 = 80$. We plot the correlations for values of α where the one-body density $\rho(x_{l,r})$ is larger than 0.01. Similarly (c) and (d) correspond to $\lambda = 6$ and $\lambda = 20$ for $V_0 = 180$. Here, the correlations of bosons in the outermost wells at $x_l(\alpha), x_r(\alpha)$ are considered.

For moderate barrier height (and smaller interaction strength), significant inter-well correlations persists for a smaller α window (note the different ranges of the panels in figure 4). However, it disappears with a further increase of α at $\lambda = 6$ [see figure 4(a)]. Further increasing the interaction strength ($\lambda = 20$) leads to left-right correlations that persist out to larger tilts α [figure 4(b)]; this behavior is a consequence of the delay of the tilt-driven localization by the increased repulsion.

In the case of larger barrier height, the left-right correlation is observed only for certain values of the tilting parameter [figures 4(c) and (d)]. Hence, by tuning the barrier height, interaction strength and tilt of the triple well, the left-right coherence can be adjusted.

3.4. Natural orbitals: variation as a function of the tilt

The behavior of the natural orbitals $\phi_i(x)$ is shown in figure 5 as a function of the tilt α for a fixed barrier height V_0 and a fixed interaction strength λ for contact interactions. Without a tilt ($\alpha = 0$), the first natural orbital $\phi_1(x)$ has three maxima which are centered at positions of the wells. The second natural orbital $\phi_2(x)$ has two maxima that are localized in the first and the third wells and the third natural orbital $\phi_3(x)$ has three maxima which are localized at the positions of the minima of the triple well similar to $\phi_1(x)$ [see figure 5(a)]. The behavior of the natural orbitals complements the nearly equal population in the three natural orbitals, i.e., the threefold fragmentation of the condensate [see figures 2(d) and 3(m)].

For $\alpha > 0$, the natural orbitals $\phi_i(x)$ adapt their shape to fit the new form of the external trapping potential. The orbitals $\phi_i(x)$ now have a single maximum and are localized independently in the three different wells [figure 5(b)]. With a further increase in α [figure 5(c)], two maxima emerge in $\phi_1(x)$ that are localized in the first and the third wells with different amplitudes. This structure of ϕ_1 is responsible for the next-to-nearest-

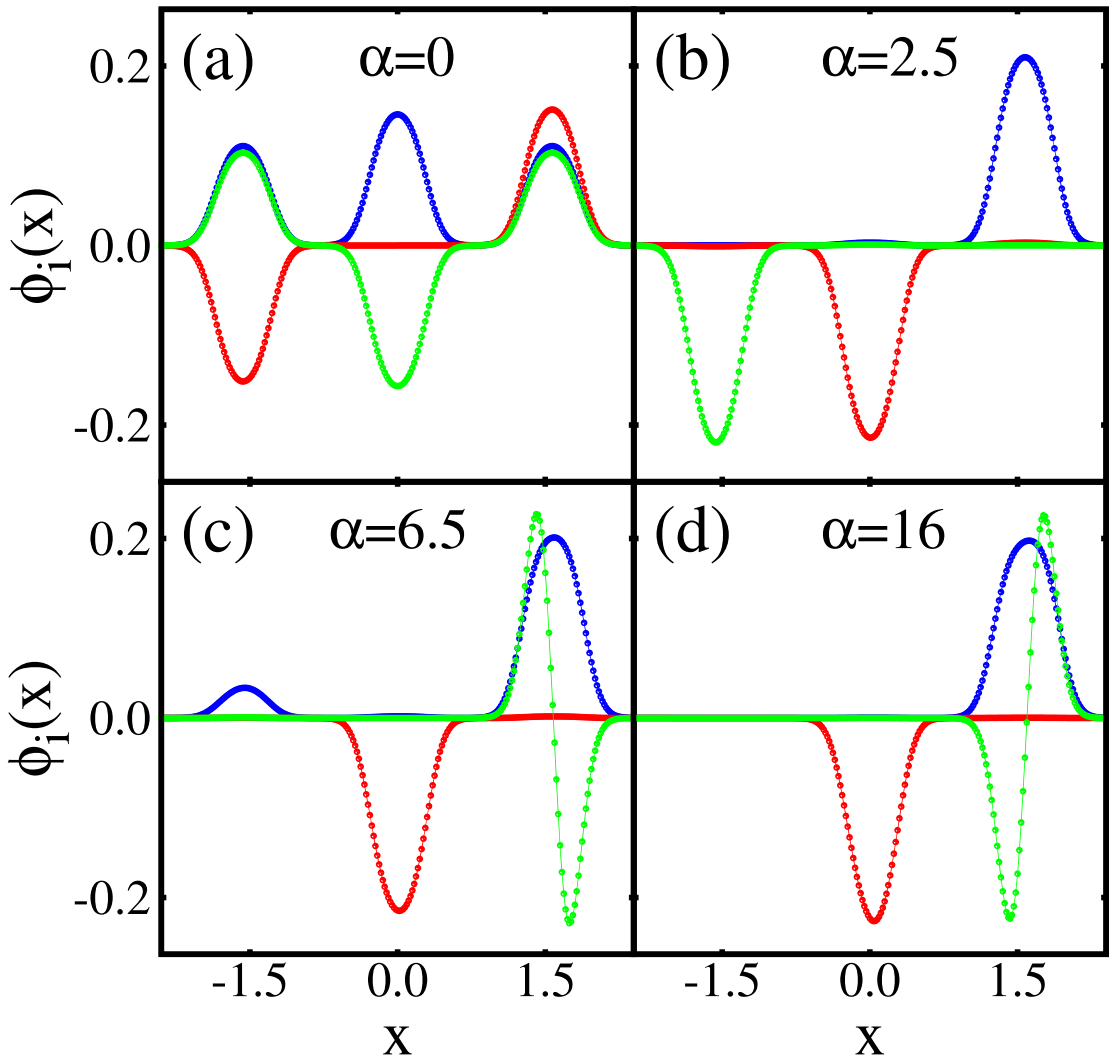

Figure 5. This figure shows the variation of natural orbitals, $\phi_i(x)$ as a function of the tilt α for $V_0 = 180$ and $\lambda = 20$ for contact interactions. It is clearly seen that the optimal MCTDHB basis does *not* correspond to site-localized Wannier or Wannier–Stark states: the Hubbard model is inapplicable. (a) Corresponds to $\alpha = 0$, (b) corresponds to $\alpha = 2.5$, (c) corresponds $\alpha = 6.5$ and (d) corresponds $\alpha = 16$. In all panels, blue lines with circles represents ϕ_1, red lines with circles represents ϕ_2 and green lines with circles represents ϕ_3. We note that, in order to assess their contribution to the one-body density $\rho^{(1)}(x, x)$, the orbitals $\phi_i(x)$ in this figure would have to be scaled by their respective occupation number n_i given in figure 2.

neighbor correlations, i.e. correlations between the first and the third wells [see figure 3(o)]. The third orbital, $\phi_3(x)$, shows a node at the center of the third well leading to a higher kinetic energy. The occupation of the third natural orbital becomes therefore the least energetically favorable. For large values of the tilt α, the natural orbitals are mainly localized in the second and the third wells [figure 5(d)].

We note here, that—similar to figure 3(o)—we also found the origin of the next-to-nearest-neighbor correlations in figure 3(j) for $V_0 = 180$, $\lambda = 6$, $\alpha = 2.5$ to be the delocalization of the first natural orbital between the left and right wells.

We also perform an analysis (footnote 5, section 2) that suggest that the Hubbard model may not be applicable. Direct comparisons of MCTDHB and the Bose–Hubbard model can be found in [64–66].

4. Conclusions

Our analysis has shown intriguing features of the first-order correlation and coherence of bosons in a tilted triple well [67, 68]. Given the ease in defining the system parameters in experimental setups with ultracold bosons, our work provides a protocol to manage the coherence of the many-body state: a variety of correlation patterns is accessible simply by appropriately choosing the interaction strength, potential depth and tilt. Superfluid states—associated with condensation—can be created either localized in one well or delocalized across all wells. Mott-insulating states—associated with fragmented systems—with a customized particle number imbalance between

distinct wells can also be prepared. The superfluid, fully coherent state and the Mott-insulating, fully incoherent phase represent extreme cases. Figure 3 illustrates how intermediate degrees of correlation can also be achieved. The counter-intuitive revivals of coherence between next-to-nearest neighboring sites seen in panels (j) and (o) of figure 3 hint that even a management of non-local correlations is possible, if the control on the tilt and interaction strength is sufficiently accurate [69]. A natural extension of our work—and in the light of recent technical developments [70]—would cover bosons with internal structure and/or embedded in an optical cavity.

We remark that, owing to its long decoherence time, the many-body state of ultracold atoms can provide a means to cache correlations and entanglement arising in quantum information processing [71]. For this purpose protocols to control and quantify correlations in the many-body state of ultracold atoms, like the one that we outlined in this work, are necessary [72]. As a further continuation of our work, we therefore also consider to quantify entanglement entropy and other quantities of relevance for quantum information processing for tilted multi-well systems.

Acknowledgments

Computational time at the HLRS Hazel Hen cluster is gratefully acknowledged. MCT acknowledges FAPESP for financial support and Hans Kessler for useful discussions. AUJL acknowledges financial support by the Austrian Science Foundation (FWF) under grant No. P 32033 and the Wiener Wissenschafts- und TechnologieFonds (WWTF) project No MA16-066.

References

[1] Anderson B P and Kasevich M A 1998 *Science* **282** 1686
[2] Greiner M, Bloch I, Mandel O, Hänsch T W and Esslinger T 2001 *Phys. Rev. Lett.* **87** 160405
[3] Greiner M, Mandel O, Esslinger T, Hänsch T W and Bloch I 2002 *Nature* **415** 39
[4] Bloch I 2005 *Nat. Phys.* **1** 23
[5] Jaksch D and Zoller P 2005 *Ann. Phys.* **315** 52
[6] Köhler T, Góral K and Julienne P S 2006 *Rev. Mod. Phys.* **78** 1311
[7] Bloch I, Dalibard J and Zwerger W 2008 *Rev. Mod. Phys.* **80** 885
[8] Chin C, Grimm R, Julienne P S and Tiesinga E 2010 *Rev. Mod. Phys.* **82** 1225
[9] Baumann K, Guerlin C, Brennecke F and Esslinger T 2010 *Nature* **464** 1301
[10] Léonard J, Morales A, Zupancic P, Esslinger T and Donner T 2017 *Nature* **543** 87
[11] Lode A U J and Bruder C 2017 *Phys. Rev. Lett.* **118** 013603
[12] Jaksch D, Bruder C, Cirac J I, Gardiner C W and Zoller P 1998 *Phys. Rev. Lett.* **81** 3108
[13] Betz T *et al* 2011 *Phys. Rev. Lett.* **106** 020407
[14] Perrin A, Bücker R, Manz S, Betz T, Koller C, Plisson T, Schumm T and Schmiedmayer J 2012 *Nat. Phys.* **8** 195
[15] Langen T, Geiger R, Kuhnert M, Rauer B and Schmiedmayer J 2013 *Nat. Phys.* **9** 640
[16] Schweigler T, Kasper V, Erne S, Mazets I, Rauer B, Cataldini F, Langen T, Gasenzer T, Berges J and Schmiedmayer J 2017 *Nature* **545** 323
[17] Chatterjee B, Tsatsos M C and Lode A U J 2019 *New J. Phys.* **21** 033030
[18] Roy R, Gammal A, Tsatsos M C, Chatterjee B, Chakrabarti B and Lode A U J 2018 *Phys. Rev.* A **97** 043625
[19] Wenz A N, Zürn G, Murmann S, Brouzos I, Lompe T and Jochim S 2013 *Science* **342** 457
[20] Murmann S, Bergschneider A, Klinkhamer V M, Zürn G, Lompe T and Jochim S 2015 *Phys. Rev. Lett.* **114** 080402
[21] Streltsov A I, Sakmann K, Alon O E and Cederbaum L S 2011 *Phys. Rev.* A **83** 043604
[22] Chatterjee B, Brouzos I, Cao L and Schmelcher P 2013 *J. Phys.* B **46** 085304
[23] Peter D, Pawlowski K, Pfau T and Rzążewski K 2012 *J. Phys.* B **45** 225302
[24] Sachdev S, Sengupta K and Girvin S M 2002 *Phys. Rev.* B **66** 075128
[25] Hiller M, Venzl H, Zech T, Oleś B, Mintert F and Buchleitner A 2012 *J. Phys.* B **45** 095301
[26] Dounas-Fraze D R, Hermundstad A M and Carr L D 2007 *Phys. Rev. Lett.* **99** 200402
[27] Penrose O and Onsager L 1956 *Phys. Rev.* **104** 576
[28] Nozières P and Saint James D 1982 *J. Phys.* **43** 1133
[29] Spekkens R W and Sipe J E 1999 *Phys. Rev.* A **59** 3868
[30] Glauber R J 1963 *Phys. Rev.* **130** 2529
[31] Pethick C J and Smith H (ed) 2002 *Bose–Einstein Condensation in Dilute Gases* (Cambridge: Cambridge University Press)
[32] Pitaevskii L P and Stringari S (ed) 2003 *Bose–Einstein Condensation* (Oxford: Clarendon)
[33] Thommen Q, Garreau J C and Zehnlé V 2002 *Phys. Rev.* A **65** 053406
[34] Larson J, Collin A and Martikainen J-P 2009 *Phys. Rev.* A **79** 033603
[35] Vermersch B and Garreau J C 2015 *Phys. Rev.* A **91** 043603
[36] Lode A U J, Sakmann K, Alon O E, Cederbaum L S and Streltsov A I 2012 *Phys. Rev.* A **86** 063606
[37] Streltsov A I, Alon O E and Cederbaum L S 2007 *Phys. Rev. Lett.* **99** 030402
[38] Alon O E, Streltsov A I and Cederbaum L S 2008 *Phys. Rev.* A **77** 033613
[39] Lode A U J 2014 *Tunneling Dynamics in Open Ultracold Bosonic Systems, Springer Theses* (Heidelberg: Springer)
[40] Nguyen J H V, Tsatsos M C, Luo D, Lode A U J, Telles G D, Bagnato V S and Hulet R G 2019 *Phys. Rev. X* **9** 011052
[41] Lode A U J 2016 *Phys. Rev.* A **93** 063601
[42] Fasshauer E and Lode A U J 2016 *Phys. Rev.* A **93** 033635
[43] Olshanii M 1998 *Phys. Rev. Lett.* **81** 938

[44] Wang Y et al 2018 Phys. Rev. Lett. 120 083601
[45] Kramer P and Saraceno M (ed) 1981 Geometry of the Time-Dependent Variational Principle (Berlin: Springer)
[46] Lode A U J, Klaiman S, Alon O E, Streltsov A I and Cederbaum L S 2014 Phys. Rev. A 89 053620
[47] Lode A U J, Chakrabarti B and Kota V K B 2015 Phys. Rev. A. 92 033622
[48] Roy R, Gammal A, Tsatsos M C, Chatterjee B, Chakrabarti B and Lode A U J 2018 Phys. Rev. A 97 043625
[49] Weiner S E, Tsatsos M C, Cederbaum L S and Lode A U J 2017 Sci. Rep. 7 40122
[50] Lode A U J and Bruder C 2016 Phys. Rev. A 94 013616
[51] Mistakidis S I, Cao L and Schmelcher P 2014 J. Phys. B: At. Mol. Opt. Phys. 47 225303
[52] Mistakidis S I, Cao L and Schmelcher P 2015 Phys. Rev. A 91 033611
[53] Mistakidis S I and Schmelcher P 2017 Phys. Rev. A 95 013625
[54] Neuhaus-Steinmetz J, Mistakidis S I and Schmelcher P 2017 Phys. Rev. A 95 053610
[55] Sakmann K (ed) 2011 Many-Body Schrödinger Dynamics of Bose–Einstein Condensates (Berlin: Springer)
[56] Sakmann K, Streltsov A I, Alon O E and Cederbaum L S 2008 Phys. Rev. A 78 023615
[57] Lode A U J, Tsatsos M C, Fasshauer E, Lin R, Papariello L, Molignini P and Lévêque C 2018 MCTDH-X: The time-dependent multiconfigurational Hartree for indistinguishable particles software (http://ultracold.org)
[58] Zöllner S, Bruun G M, Pethick C J and Reimann S M 2011 Phys. Rev. Lett. 107 035301
[59] Zöllner S 2011 Phys. Rev. A 84 063619
[60] Fischer U R, Lode A U J and Chatterjee B 2015 Phys. Rev. A 91 063621
[61] Chatterjee B and Lode A U J 2018 Phys. Rev. A 98 053624
[62] Zöllner S, Meyer H-D and Schmelcher P 2008 Phys. Rev. Lett. 100 040401
[63] Lode A U J, Streltsov A I, Sakmann K, Alon O E and Cederbaum L S 2012 Proc. Natl Acad. Sci. 109 13521
[64] Sakmann K, Streltsov A I, Alon O E and Cederbaum L S 2010 Phys. Rev. A 82 013620
[65] Sakmann K, Streltsov A I, Alon O E and Cederbaum L S 2009 Phys. Rev. Lett. 103 220601
[66] Sakmann K, Streltsov A I, Alon O E and Cederbaum L S 2011 New J. Phys. 13 043003
[67] Pielawa S, Kitagawa T, Berg E and Sachdev S 2011 Phys. Rev. B 83 205135
[68] Meinert F, Kirilov M J, Lauber K, Weinmann P, Daley A J and Nägerl H-C 2013 Phys. Rev. Lett. 111 053003
[69] Molignini P, Papariello L, Lode A U J and Chitra R 2018 Phys. Rev. A 98 053620
[70] Lode A U J et al 2018 New J. Phys. 20 055006
[71] Bloch I 2008 Nature 453 1016
[72] Cramer M, Bernard A, Fabbri N, Fallani L, Fort C, Rosi S, Caruso F, Inguscio M and Plenio M B 2013 Nat. Commun. 4 2161